



**HAL**  
open science

# Influence of the polarization anisotropy on the linewidth enhancement factor and reflection sensitivity of 1.55- $\mu\text{m}$ InP-based InAs quantum dash lasers

Bozhang Dong, Jianan Duan, Chen Shang, Heming Huang, Alfred Bewindin Sawadogo, Dahwan Jung, Yating Wan, John Bowers, Frédéric Grillot

## ► To cite this version:

Bozhang Dong, Jianan Duan, Chen Shang, Heming Huang, Alfred Bewindin Sawadogo, et al.. Influence of the polarization anisotropy on the linewidth enhancement factor and reflection sensitivity of 1.55-  $\mu\text{m}$  InP-based InAs quantum dash lasers. *Applied Physics Letters*, 2019, 115 (9), pp.091101. 10.1063/1.5110768 . hal-02307297

HAL Id: hal-02307297

<https://telecom-paris.hal.science/hal-02307297v1>

Submitted on 7 Oct 2019

**HAL** is a multi-disciplinary open access archive for the deposit and dissemination of scientific research documents, whether they are published or not. The documents may come from teaching and research institutions in France or abroad, or from public or private research centers.

L'archive ouverte pluridisciplinaire **HAL**, est destinée au dépôt et à la diffusion de documents scientifiques de niveau recherche, publiés ou non, émanant des établissements d'enseignement et de recherche français ou étrangers, des laboratoires publics ou privés.

# Influence of the polarization anisotropy on the linewidth enhancement factor and reflection sensitivity of 1.55- $\mu\text{m}$ InP-based InAs quantum dash lasers

Cite as: Appl. Phys. Lett. **115**, 091101 (2019); <https://doi.org/10.1063/1.5110768>

Submitted: 21 May 2019 . Accepted: 07 August 2019 . Published Online: 26 August 2019

B. Dong , J. Duan , C. Shang, H. Huang, A. B. Sawadogo, D. Jung, Y. Wan, J. E. Bowers, and F. Grillot



View Online



Export Citation



CrossMark

## Applied Physics Letters

Mid-IR and THz frequency combs  
special collection

Read Now!

AIP  
Publishing

# Influence of the polarization anisotropy on the linewidth enhancement factor and reflection sensitivity of 1.55- $\mu\text{m}$ InP-based InAs quantum dash lasers

Cite as: Appl. Phys. Lett. **115**, 091101 (2019); doi: [10.1063/1.5110768](https://doi.org/10.1063/1.5110768)

Submitted: 21 May 2019 · Accepted: 7 August 2019 ·

Published Online: 26 August 2019



View Online



Export Citation



CrossMark

B. Dong,<sup>1</sup>  J. Duan,<sup>1</sup>  C. Shang,<sup>2</sup> H. Huang,<sup>1</sup> A. B. Sawadogo,<sup>1</sup> D. Jung,<sup>2,3</sup> Y. Wan,<sup>4</sup> J. E. Bowers,<sup>2,4,5</sup> and F. Grillot<sup>1,6,a)</sup>

## AFFILIATIONS

<sup>1</sup>LTCl, Télécom Paris, Institut Polytechnique de Paris, 46 rue Barrault, Paris 75013, France

<sup>2</sup>Institute for Energy Efficiency, University of California Santa Barbara, 2314 Phelps Hall, Santa Barbara, California 93106, USA

<sup>3</sup>Center for Opto-Electronic Materials and Devices, Korea Institute of Science and Technology, Seoul 02792, South Korea

<sup>4</sup>Department of Electrical and Computer Engineering, University of California Santa Barbara, Santa Barbara, California 93106, USA

<sup>5</sup>Materials Department, Engineering II Building, 1355, University of California Santa Barbara, Santa Barbara, California 93106, USA

<sup>6</sup>Center for High Technology Materials, University of New-Mexico, 1313 Goddard St SE, Albuquerque, New Mexico 87106, USA

<sup>a)</sup>Electronic mail: [frederic.grillot@telecom-paristech.fr](mailto:frederic.grillot@telecom-paristech.fr)

## ABSTRACT

This work investigates the effect of the polarization anisotropy on the linewidth enhancement factor and the reflection sensitivity of InAs/InP quantum dash semiconductor lasers. The results show that the small linewidth enhancement factor and high stability against external optical feedback are obtained for nanostructures oriented perpendicular to the cavity axis as opposed to those oriented parallel to the cavity axis. Effective simulations on the critical feedback level of these two lasers are also in agreement with experimental results. Such anisotropy is attributed to the polarization dependence of the transition matrix element in these quantum nanostructures.

Published under license by AIP Publishing. <https://doi.org/10.1063/1.5110768>

High performance semiconductor lasers are important for data-com and optical communications.<sup>1–3</sup> Reducing the number of degrees of freedom leads to the formation of nanostructures with low dimensionality such as the quantum dot (QDot) or quantum dash (QDash).<sup>4</sup> On the first hand, ideal QDot systems exhibit an atomlike density of states, which is of paramount importance for the fabrication of optical transmitters with high thermal stability, low threshold current density, and a large level of reflection insensitivity.<sup>5,6</sup> On the other hand, QDashes are elongated nanostructures with strong anisotropy, exhibiting electronic properties rather close to quantum wires.<sup>7</sup> In particular, previous works have shown that InAs/InP quantum confined devices emitting at 1550 nm and including InAs QDot or QDash nanostructures as a gain media grown are very promising for various applications requiring frequency comb generation,<sup>3,8,9</sup> low-phase noise operation,<sup>10</sup> and passive mode-locking.<sup>11</sup> However, compared to QDots, the strong anisotropy of QDash leads to a polarization dependence with respect to the laser cavity axis that needs to be carefully

taken into account for engineering photonic devices with the best performance.<sup>12</sup> To this end, this Letter reports the influence of the InAs/InP QDash polarization on the linewidth enhancement factor (LEF) and the impact of this anisotropy on the reflection sensitivity to external reflections. The LEF is known to be a vital parameter in semiconductor laser physics, which influences many characteristics and performance such as the spectral linewidth and the frequency chirp under direct modulation and on the top of that the dynamical response to external optical feedback.<sup>13</sup> A semiconductor laser's sensitivity to parasitic reflections is directly tied to its LEF, and hence, the smaller the LEF, the better the stability as recently demonstrated with epitaxial QDot lasers grown on silicon.<sup>6,14</sup> The last point is of particular importance for isolator-free photonic integrated circuits which require expensive and bulky optical isolators, hence leading to a large increase in the device footprint for on-chip integration.

In this work, we show that the control of the polarization dependence of the QDash is directly connected with the resulting dynamical

properties of the semiconductor lasers operating under optical feedback. Thus, with QDash oriented perpendicular to the cavity, a smaller LEF is obtained, which transforms by far into a higher stability against optical feedback. The latter is analyzed through the critical feedback level, driving the route to chaos and giving the maximum feedback level that can be tolerated for a floor-free operation in a high-speed communication system. Here, the critical feedback level is found to be up-shifted by 11-dB with QDash oriented perpendicular to the cavity as opposed to those grown parallel to the cavity. Overall, the letter probes the importance of the anisotropy of the QDash material and gives highlights for engineering future InP-based InAs QDash lasers with high dynamical performance.

The laser structures under study are grown on an n-InP (001) substrate using the InAs QDash as the active region. Figure 1(a) depicts the atomic force microscopy (AFM) image of the QDash morphology. The QDashes are elongated in the  $[1\bar{1}0]$  direction due to a higher indium surface diffusion in the  $[1\bar{1}0]$  direction with an average length of 200 nm. The polarization of dashes is then determined by the included angle between the axis of dashes and the axis of cavity. Figure 1(b) displays the cross-sectional transmission electron microscopy image of the QDash lasers. The structure was grown at a constant temperature of 500 °C except for the QDash active region, which was grown at 485 °C. Using a total InAs deposition of 3.25 monolayer (ML), a V/III ratio of 18, and a growth rate of 0.4 ML/s, we have obtained better photoluminescence (PL) characteristics. Postnucleation growth interruption was also introduced to further tune the wavelength at an  $As_2$  overpressure of  $1 \times 10^{-6}$  Torr for 60 s. Let us note that the PL FWHM is about 100 meV for QDash nanostructures (not shown here) against 30 meV for QDots.<sup>6</sup> The detailed epi-structure of the laser is shown in Fig. 1(c). Five layers of dashes spaced by a 40 nm thick p-InGaAlAs separated confinement heterojunction (SCH) spacer were grown within the active region to provide the p-modulation at  $5 \times 10^{17} \text{ cm}^{-3}$ . The p-doping helps to enhance the thermal stability of the laser, considering that QDot lasers suffer from thermal broadening of carriers, especially from holes due to their heavier effective mass and consequent tightly spaced energy levels.<sup>15</sup> The former work also revealed that the QDot laser with doping could improve the differential gain and decrease LEF, as the thermal broadening decreases the QDot

ground state gain.<sup>16,17</sup> The SCH layers on both sides of the active region were 150 nm thick  $In_{0.527}Ga_{0.234}Al_{0.239}As$ . The bottom and top cladding layers used to protect the structure were formed by n- and p-type  $In_{0.523}Al_{0.477}As$  with different doping rates whose lattices were well matched to the InP substrate at the bottom. Between the SCH layers and the cladding layers, 50 nm digital quaternary InGaAlAs alloys were used to grade the bandgap from  $In_{0.523}Al_{0.477}As$  to  $In_{0.527}Ga_{0.234}Al_{0.239}As$ . Both the grading and the SCH layers are symmetric at the top and the bottom of the QDash active region. At the top of the structure, after another 100 nm InGaAlAs digital alloy grading layer, the structure was completed with a 100 nm thick p-doped  $In_{0.532}Ga_{0.468}As$  contact layer. In what follows, lasers with different orientations of QDash were compared. The laser with QDash parallel (perpendicular) to the cavity axis has a ridge waveguide width of 2.5  $\mu\text{m}$  (4  $\mu\text{m}$ , respectively). Finally, both the devices have a cavity length of 1.25 mm and are as-cleaved with the reflectivity  $R$  at 32%. Let us stress that although the ridge waveguide widths are slightly different, it is shown in the following that such a small difference does not impact the feedback dynamics, which remains fundamentally driven by the cavity photon round trip time and the LEF. All the measurements described hereinafter are performed at room temperature (293 K).

Figure 2 depicts the light current characteristics, and the inset shows the corresponding optical spectra measured at  $1.5 \times I_{th}$  of the two lasers with dashes oriented parallel (red) to the cavity axis and with dashes oriented perpendicular (blue) to the cavity axis; correlative studies could also be found in previous works.<sup>18,19</sup> Both the devices display lasing emission on fundamental ground state transition at either 1576 nm with QDash oriented parallel to the cavity axis or 1596 nm for those oriented perpendicular to the cavity axis. The wavelength shift can be attributed to the different transition matrix element for heavy hole (HH) and light hole (LH) states in QDash structures.<sup>12</sup> Indeed, due to the compressive strain in dashes, the conduction band-to-LH band (C-LH) transitions have the largest oscillator strength when the electric field is perpendicular to dash axis, whereas the conduction band-to-HH band (C-HH) transitions hold the dominant position when the electric field is in the plane of dash axis. Therefore, the narrower C-HH bandgap eventually results in the wavelength redshift at the peak modal gain when the dashes rotated from parallel to

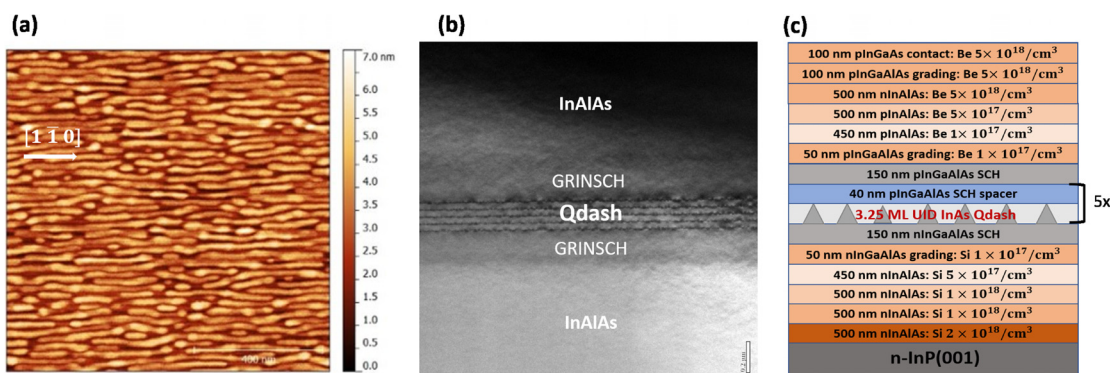


**FIG. 1.** (a)  $1 \times 1 \mu\text{m}^2$  AFM image of the QDash morphology. The QDashes are highly elongated in the  $[1\bar{1}0]$  direction due to asymmetric surface diffusion of indium adatoms. The average height and width are about 7 and 20 nm, respectively. (b) Cross-sectional TEM image of the  $[1\bar{1}0]$  surface at 9000 $\times$  magnification, showing the 5 layers of QDash. The electron beam energy was 200 keV. (c) Schematic of the laser epi-structure with 5 layers of p-doping QDash in the active region.

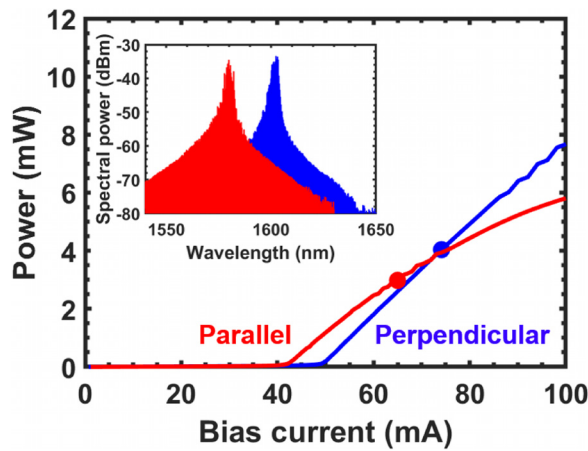


FIG. 2. Light-current characteristics and (inset) the optical spectra measured at  $1.5 \times I_{th}$  for QDash oriented parallel (red) and perpendicular (blue) to the cavity axis.

perpendicular to the cavity axis.<sup>12</sup> On the other hand, the threshold current  $I_{th}$  of the laser including dashes oriented perpendicular to the cavity axis is 49 mA, whereas it is reduced down to 43 mA otherwise. The larger threshold current observed with QDash oriented perpendicular to the cavity axis can be attributed to the wider ridge width and to the higher optical loss caused by higher free carrier absorption that is induced by the large number of holes in the dashes.<sup>12,20</sup>

As described in previous works,<sup>6,21</sup> the modal gain and the sub-threshold LEF are together extracted from the amplified spontaneous emission (ASE). In the latter, the wavelength red-shift due to thermal effects, measured by varying the pump current right above threshold, must be properly subtracted from the wavelength blue-shift measured below threshold. In the experiments, a continuous-wave (CW) current source was applied to bias the lasers to avoid irregular optical spectral line shapes, hence improving the accuracy of LEF extraction. Emission from the QDash lasers is coupled into a 20 pm high resolution optical spectrum analyzer via an antireflection (AR) coated lensed fiber. An isolator is placed after the laser in order to eliminate any source of optical feedback from the experimental set-up. The device temperature is carefully monitored throughout the measurement.

Figure 3(a) displays the net modal gain under different bias currents for the laser with QDash oriented parallel to the cavity axis (red) and with QDash oriented perpendicular to the cavity axis (blue). On the one hand, the position of the peak modal gain for dashes perpendicular to the cavity axis is shifted by 15 nm to a longer wavelength with respect to the peak position of modal gain for dashes parallel to the cavity axis. On the other hand, the peak value of net modal gain is about  $9 \text{ cm}^{-1}$ , which is expected since the cavity lengths are identical for both lasers. However, it has to be noted that the modal gain including internal loss is expected to be larger for lasers with QDashes oriented perpendicular to the cavity axis than that for lasers with QDashes along the cavity.<sup>12</sup> Figure 3(b) displays the spectral dependence of the LEFs extracted at threshold for both cases. For the whole wavelength range, the LEF values are always found to be larger for the parallel QDash laser. For instance, at the gain peak (marked by black dashed lines), the LEF is 2.5 for the laser with QDash along the cavity axis

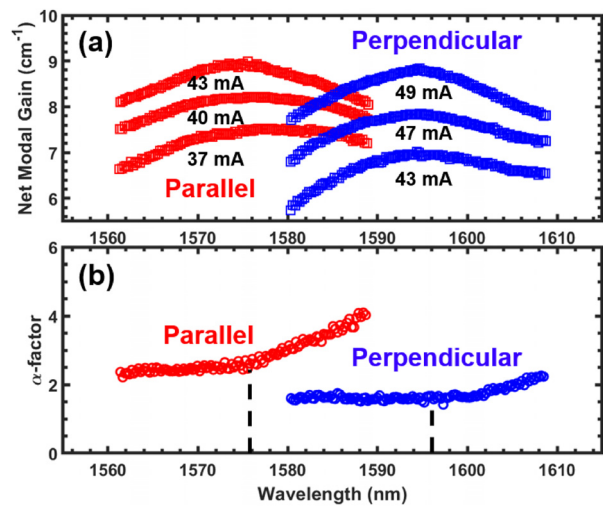


FIG. 3. (a) Net modal gain and (b) LEF at threshold as a function of the photon wavelength for the laser with QDash oriented parallel (red) and perpendicular (blue) to the cavity axis.

against 1.5 otherwise. This effect is in agreement with other research,<sup>12</sup> and as aforementioned, this difference results from the orientation dependence of the transition matrix element for the QDash active media. Let us stress that a previous work showed that for epitaxial QDot lasers on silicon, the wider the ridge, the larger the LEF.<sup>17</sup> In the case of QDash elongated nanostructures, the situation is different due to the polarization anisotropy. Indeed, although the laser with dashes perpendicular to the cavity axis has a wider ridge, the C-HH transitions contribute to decreasing the LEF as shown in Fig. 3(b).

The experimental setup used for investigating the optical feedback is shown in Fig. 4. Laser emission is coupled by antireflection (AR)-coated lens-end fiber and divided into two paths: a feedback path (with 90% coupled power) and a detection path (with 10% coupled power). A backreflector (BKR) combined with a variable optical attenuator is wired in the feedback path in order to reflect the light back to the laser cavity and change the feedback strength  $r_{ext}$ , which is defined as the ratio between the power return to the laser cavity and the free-space emitting power of laser. The losses from the fiber coupling and in the fiber setup are taken into account to accurately calculate  $r_{ext}$ . A polarization controller is inserted in the external cavity to compensate for the fiber dispersion and thus maximize the effects of the optical feedback. An isolator in the detection path is applied to prevent additional feedback from the setup. The remaining coupled light is then transferred to an optical switch (SWT), where the signal would

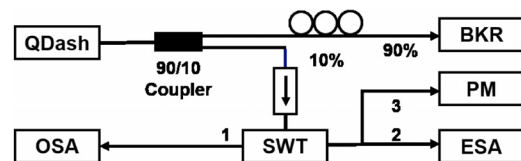


FIG. 4. Schematic of the experimental setup used for investigating optical feedback. QDash, QDash laser diode; BKR, backreflector; SWT, optical switch; OSA, optical spectrum analyzer; ESA, electrical spectrum analyzer; PM, powermeter.

be swapped between the powermeter (PM) and the optical and electrical spectrum analyzers (OSAs and ESAs) for further analysis. In the experiments, only the long delay regime is studied (7 m-long external cavity), which means that the relaxation oscillation frequency of the laser is well-beyond that of the external cavity.

Figure 5 displays the optical feedback dynamics at  $1.5 \times I_{th}$  for the two QDash lasers by varying  $r_{ext}$  from  $-60$  dB to  $-7$  dB. The left column corresponds to the case of QDash along the cavity axis, whereas the right one is obtained for nanostructures perpendicular to the cavity axis. For both lasers, the dynamics is monitored in both the radio frequency (RF) [Figs. 5(a) and 5(b)] and optical [Figs. 5(c) and 5(d)] domains. The critical feedback level  $r_{crit}$  corresponding to the occurrence of the first Hopf bifurcation is represented by the green dashed line above. It is used as the criteria that guarantee a stable utilization of the laser in a communication system. Experiments unveil that the critical feedback level is at  $-34$  dB for the parallel QDash laser against  $-23$  dB for the perpendicular one. Such an 11 dB difference directly results from the lower LEF associated with the polarization anisotropy of the dashes. As shown in Figs. 5(c) and 5(d), above the bifurcation, broadening of the longitudinal modes is observed without ambiguity for both lasers. This phenomenon is also confirmed in the RF domain [Figs. 5(a) and 5(b)] with the appearance of multiple frequencies, hence confirming that each laser transitions from a steady-state to a quasiperiodic regime that can further evolve into chaotic oscillations. Recent work on  $1.3 \mu\text{m}$  QDot lasers showed a more uniform array of emitters, and hence, a narrower PL and a larger reduction of LEF (to  $\sim 0$ ) can be totally reflection insensitive without any chaotic oscillations.<sup>6</sup> Here, the critical feedback level of the QDash lasers can be clearly identified for both orientations. As a conclusion, such an 11 dB enhancement of the critical feedback level combined with the stability of the longitudinal modes under feedback demonstrates that the laser with QDash oriented perpendicular to the cavity axis is more stable against parasitic reflections.

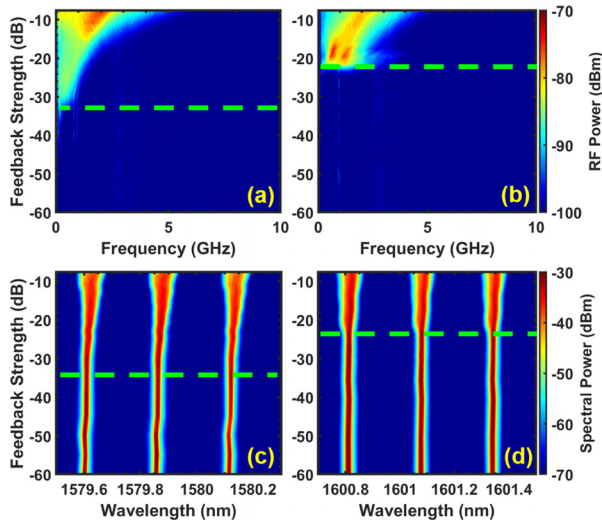


FIG. 5. (a) RF spectral and (c) Optical mappings of the laser with QDash oriented parallel to the cavity axis as a function of the feedback strength at  $1.5 \times I_{th}$ ; (b) RF spectral and (d) Optical mappings of the laser with QDash oriented perpendicular to the cavity axis as a function of the feedback strength at  $1.5 \times I_{th}$ . The critical feedback level  $r_{crit}$  is marked by the green dashed lines.

It is known that both the LEF and the damping factor  $\gamma$  of the relaxation oscillations affect the reflection sensitivity of any semiconductor laser. An approximate relationship for getting the first Hopf bifurcation, namely, the critical feedback level  $r_{crit}$  of a semiconductor laser having a LEF greater than the unity, is given by the following relationship:

$$r_{crit} = \frac{\gamma^2 \tau_L^2}{16C^2} f(\alpha), \tag{1}$$

with  $f(\alpha) = (1 + \alpha^2)^{-1}$ ,  $\tau_L$  being the round trip time in the laser cavity,  $C = (1 - R)/2\sqrt{R}$  the coupling strength from the laser cavity to the external cavity, and  $\alpha$  the LEF. Figure 6 shows the evolution of  $r_{crit}$  as a function of  $\gamma$  for both parallel (red) and perpendicular (blue) QDash lasers. In the simulations, the LEF values measured at threshold for both QDash lasers are increased by 15% (estimated at  $1.5 \times I_{th}$ ) in order to reflect the LEF balloons beyond the laser's threshold.<sup>22</sup> By doing so, Fig. 6 shows that the critical feedback level experimentally displayed in Fig. 5 can be retrieved from the simulations. The values of  $-23$  dB and  $-34$  dB (filled circles) correspond to the damping rate on the order of 10 GHz, respectively, which is in agreement with previous measurements performed on similar QDash material systems.<sup>22,23</sup> On the other hand, the measured 11 dB enhancement in  $r_{crit}$  for QDashes perpendicular to the cavity axis confirms its higher damping factor and larger  $r_{crit}$ . Despite that, it is, however, important to stress that (1) holds under many approximations and might not always reflect the first Hopf bifurcation point. A previous work showed that the level of proximity between the relation given the first Hopf bifurcation derived from the Jacobian matrix and that from Eq. (1) can be expressed as follows:<sup>24</sup>

$$\beta = \frac{\cos^2[\phi_0 - \arctan(\alpha)]}{4(1 - R)^2}, \tag{2}$$

with  $\phi_0$  being the phase of the feedback wave returning into the cavity. Figure 7 displays the evolution of the  $\beta$ -factor as a function of the LEF and  $\phi_0$ . The two vertical dashed lines correspond to the region, where the  $\beta$ -factor is the largest, meaning that the discrepancy between the two models is minimum. Taking an external cavity length of 7 m combined with LEF values greater than unity could make the value of

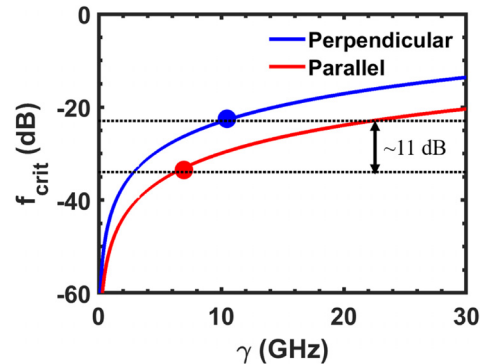
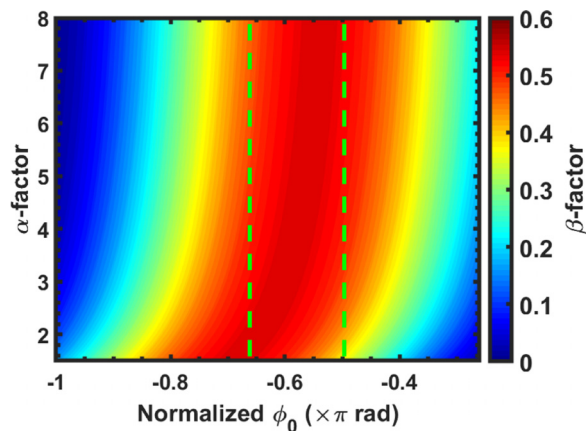


FIG. 6. The simulated critical feedback level  $r_{crit}$  as a function of the damping factor  $\gamma$  for both QDash lasers oriented either parallel (red) and perpendicular (blue) to the cavity axis. Black dashed lines at  $-23$  dB and  $-34$  dB indicate the measured  $r_{crit}$  of  $1.5 \times I_{th}$  in Fig. 5.



**FIG. 7.** The calculated  $\beta$ -factor as a function of the LEF and  $\phi_0$ . Green dashed lines are located in the interval of  $\phi_0$ , which improves the approximate model [Eq. (1)] accuracy up to 0.5 (−3 dB).

phase  $\phi_0$  fall into the interval between  $-0.65 \times \pi$  and  $-0.5 \times \pi$  rad. In such a way, the  $\beta$ -factor quickly stabilizes to its maximum value of 0.5 (−3 dB), meaning that the use of Eq. (1) is reliable for predicting the first Hopf bifurcation of QDash lasers under study.

To summarize, this work demonstrates the importance of the dash orientation in the optical properties of the laser gain medium. Considering QDash perpendicular to the cavity axis, those initial results show that the LEF is reduced by a factor of 1.5 and the critical feedback is increased by 11 dB;<sup>25</sup> such results are also approved by simulations. This is important for a stable utilization of such a laser in a communication system. Further work will investigate the influence of the inhomogeneous broadening of the QDash size dispersion on the LEF and the reflection sensitivity.

The authors acknowledge the financial support of ARPA-E (Fresco No. DE-AR0001042) and the Institut Mines Télécom, France.

## REFERENCES

- <sup>1</sup>R. Helkey, J. F. Buckwalter, A. Saleh, and J. E. Bowers, *IEEE J. Sel. Top. Quantum Electron.* **25**, 8300215 (2019).
- <sup>2</sup>K. Kikuchi, *J. Lightwave Technol.* **34**, 157 (2016).
- <sup>3</sup>Y. Mao, J. Liu, Z. Lu, C. Song, and P. J. Poole, in *Optical Fiber Communication Conference (OSA, 2019)*.
- <sup>4</sup>J. C. Norman, D. Jung, Z. Zhang, Y. Wan, S. Liu, C. Shang, R. W. Herrick, W. W. Chow, A. C. Gossard, and J. E. Bowers, *IEEE J. Quantum Electron.* **55**, 1 (2019).
- <sup>5</sup>G. Eisenstein and D. Bimberg, *Green Photonics and Electronics* (Springer, 2017).
- <sup>6</sup>J. Duan, H. Huang, B. Dong, D. Jung, J. C. Norman, J. E. Bowers, and F. Grillot, *IEEE Photonics Technol. Lett.* **31**, 345–348 (2019).
- <sup>7</sup>M. Gioannini, *IEEE J. Quantum Electron.* **42**, 331 (2006).
- <sup>8</sup>V. Vujicic, C. Calo, R. Watts, F. Lelarge, C. Browning, K. Merghem, A. Martinez, A. Ramdane, and L. P. Barry, *IEEE J. Sel. Top. Quantum Electron.* **21**, 1101508 (2015).
- <sup>9</sup>C. Zhang, D. Liang, G. Kurczveil, A. Descos, and R. Beausoleil, in *International Semiconductor Laser Conference (IEEE, 2018)*, p. 79.
- <sup>10</sup>A. Becker, V. Sichkovskyi, M. Bjelica, A. Rippien, F. Schnabel, M. Kaiser, O. Eyal, B. Witzigmann, G. Eisenstein, and J. Reithmaier, *Appl. Phys. Lett.* **110**, 181103 (2017).
- <sup>11</sup>S. Meinecke, L. Drzewietzki, C. Weber, B. Lingnau, S. Breuer, and K. Lüdge, *Sci. Rep.* **9**, 1783 (2019).
- <sup>12</sup>A. A. Ukhanov, R. H. Wang, T. J. Rotter, A. Stintz, L. F. Lester, P. G. Eliseev, and K. J. Malloy, *Appl. Phys. Lett.* **81**, 981 (2002).
- <sup>13</sup>A. Liu, T. Komljenovic, M. Davenport, A. Gossard, and J. Bowers, *Opt. Express* **25**, 9535 (2017).
- <sup>14</sup>H. Huang, J. Duan, D. Jung, A. Y. Liu, Z. Zhang, J. Norman, J. E. Bowers, and F. Grillot, *J. Opt. Soc. Am. B.* **35**, 2780 (2018).
- <sup>15</sup>M. T. Crowley, N. A. Naderi, H. Su, F. Grillot, and L. F. Lester, in *Advances in Semiconductor Lasers*, edited by J. J. Coleman, A. Bryce, and C. Jagadish (Academic Press, 2012), pp. 371–417.
- <sup>16</sup>Z. Zhang, D. Jung, J. C. Norman, P. Patel, W. W. Chow, and J. E. Bowers, *Appl. Phys. Lett.* **113**, 061105 (2018).
- <sup>17</sup>J. Duan, H. Huang, D. Jung, Z. Zhang, J. Norman, J. E. Bowers, and F. Grillot, *Appl. Phys. Lett.* **112**, 251111 (2018).
- <sup>18</sup>S. Hein, P. Podemski, G. Sk, J. Misiewicz, P. Ridha, A. Fiore, G. Patriarche, S. Hfling, and A. Forchel, *Appl. Phys. Lett.* **94**, 241113 (2009).
- <sup>19</sup>R. H. Wang, A. Stintz, P. M. Varangis, T. C. Newell, H. Li, K. J. Malloy, and L. F. Lester, *IEEE Photonics Technol. Lett.* **13**, 767–769 (2001).
- <sup>20</sup>G. J. Letal, J. G. Simmons, J. D. Evans, and G. P. Li, *IEEE J. Quantum Electron.* **34**, 512 (1998).
- <sup>21</sup>M. Osinski and J. Buus, *IEEE J. Quantum Electron.* **23**, 9 (1987).
- <sup>22</sup>N. A. Naderi, M. Pochet, F. Grillot, N. B. Terry, V. Kovanis, and L. F. Lester, *IEEE J. Sel. Top. Quantum Electron.* **15**, 563 (2009).
- <sup>23</sup>T. Sadeev, D. Arsenijević, and D. Bimberg, *Appl. Phys. Lett.* **109**, 161104 (2016).
- <sup>24</sup>Q. Zou and S. Azouigui, *Semiconductor Laser Diode Technology and Applications* (Intech, 2012).
- <sup>25</sup>S. Azouigui, B. Dagens, F. Lelarge, J. Provost, D. Make, O. L. Gouezigou, A. Accard, A. Martinez, K. Merghem, F. Grillot, O. Dehaese, R. Piron, S. Loualiche, Q. Zou, and A. Ramdane, *IEEE J. Sel. Top. Quantum Electron.* **15**, 764 (2009).